NUMERICAL AND EXPERIMENTAL INVESTIGATION INTO THE ACCURACY OF THE FAN SCALING LAWS APPLIED TO LARGE DIAMETER AXIAL FLOW FANS

Ockert P.H. AUGUSTYN[1], Sybrand J. VAN DER SPUY[2], Theodor.W. von BACKSTRÖM[2]

[1] *Eskom Holdings SOC, Enterprises Park, Simba road, Sandton, 2191, South Africa*

[2] *Department of Mechanical and Mechatronic Engineering, Stellenbosch University, Joubert Street, Stellenbosch, 7600, South Africa*

SUMMARY

The cooling effectiveness of air-cooled steam condenser (ACSC) units is impacted by the performance of the large diameter axial flow cooling fans, which ultimately affects the overall efficiency of the power plant. Due to the large diameters of these fans, performance tests are carried out at test facilities with smaller, standardized diameters and measuring equipment. The performance of the large scale fans can be predicted based on the small scale test results using the similarity laws and scale-up formulae. This paper details the results of small scale experimental tests and numerical simulations that were performed on a pair of 1.25 m diameter axial flow fans. Full scale, 10.360 m, diameter simulations of the same axial flow fans were subsequently performed and compared to the experimental results that were scaled up using the fan scaling laws. The results show that the scaled fan results are within 5% of the experimental results.

INTRODUCTION

The bulk of South Africa's electrical power is produced by coal-fired power plants. Cooling for these power generating cycles has become an increasingly complex problem due to the limited availability and rising cost of water in the vicinity of plant sites [1]. Wet-cooled power stations are generally preferred because of their higher thermal efficiencies, although an adequate supply of suitable water is required. Due to the fact that the power stations currently under construction in South Africa are located in coal rich, water scarce regions, wet-cooled systems are not feasible from an environmental and economic perspective. Consequently the focus has shifted towards dry-cooled systems, specifically direct dry-cooled systems using large arrays of axial flow fans in air-cooled steam condensers (ACSC).

The performance of ACSC units, as part of the power generation cycle, impacts the overall efficiency of the plant. This is explained by considering the Rankine cycle shown on the T-s

diagram in Figure 1. Heat is added to the cycle (q_{in}) in order for the water to reach superheated steam condition (point 3). The pressure at this point is independent of the performance of the turbine or cooling system. The superheated steam then passes through the turbine and work is done. The amount of work done by the turbine is determined by the total enthalpy drop across the turbine, and, of course, by the turbine efficiency. The pressure at the turbine's outlet is referred to as the system's back pressure. An increase in the back pressure will consequently result in a decrease in the net work output ($W_{net,out}$) of the system.

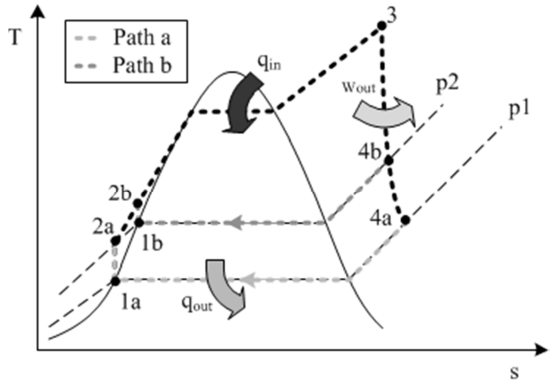

Figure 1 - Rankine energy cycle

The ACSC cooling system will always be able to reject the heat from the turbine. However, it is well-known that the condensing pressure is fixed by the cold sink temperature. So, the performance of the actual thermodynamic cycle is influenced by adverse weather conditions. In particular, an increase of the operating temperature results in an increased back pressure and the system will subsequently operate as indicated by path b (see, Fig. 1) Therefore, inadequate cooling by the ACSC units will adversely affect the efficiency of the power plant. Factors which influence the performance (ability to reject heat) of an ACSC include the ambient dry-bulb temperature, air density, finned tube temperature and volume flow rate delivered by the fans [2]. The heat rejection rate of ACSC units is greatly influenced by the volume flow rate through the heat exchanger and recirculation forming below the cooling platform [3,4].

The volume flow rate delivered by a cooling fan is determined by the location of the fan's operating point. The operating point is obtained from the intersection between the fan static pressure curve and the pressure losses curve of the ACSC unit [1]. The standard fan performance curves of the large diameter fans used in ACSC units, cannot be determined from experiments. Large diameter axial cooling fans are typically more than 10 m in diameter, which makes them impractical to test or monitor on site. Therefore, the performance specifications of these large axial fans are based on scaled fan test results. Meyer and Kröger [5] performed a numerical investigation on the accuracy of using the fan scaling laws to predict the performance of a large 9 m diameter axial flow fan. They used a simplified numerical model, referred to as the actuator disc, to represent the large diameter axial flow fan and compared the simulated results to experimental results scaled from a diameter of 1.542 m to 9 m. Meyer and Kröger found that the fan static pressure rise and fan shaft power consumption determined using the scaling laws are 3 and 4% lower respectively, compared to the numerical values. They also found that the fan static efficiency for the two sets of results are "near identical".

Following on the work of Meyer and Kröger, a concerted effort had been made to improve the modelling of an axial flow fan using computational fluid dynamics (CFD). In a study by Augustyn [2], fully detailed CFD simulations were carried out for a 1.25 m axial fan in a BS 848 (type A) fan test facility using *ANSYS Fluent*. A "type A" facility specifies a large inlet and open outlet. The results of the simulations were validated by experiments and good agreement was obtained.

It was therefore decided to use CFD to investigate the scaled modelling of a large diameter axial flow fan, typically used in ACSCs. The CFD analyses would replicate the testing of two different 1.25 m diameter axial flow fans in a BS 848 (type A) test facility. The CFD analyses would then be repeated for the same two axial flow fans but with the geometry scaled to a diameter of 10.36 m. The large diameter CFD results would then be compared to the scaled experimental results using the fan scaling laws. Although a number of authors have been investigating the scaling of fan test results [6], this investigation focussed specifically on the application of the fan scaling laws to large diameter fans.

FAN SCALING LAWS

The fan scaling laws are derived using the process of dimensional analysis. The fan laws are listed by Meyer and Kröger [5] as:

$$\frac{\dot{V}'}{\dot{V}} = \left(\frac{N'}{N}\right)\left(\frac{D'}{D}\right)^3 \tag{2}$$

$$\frac{\Delta p'_{sF}}{\Delta p_{sF}} = \left(\frac{N'}{N}\right)^2\left(\frac{D'}{D}\right)^2\left(\frac{\rho'}{\rho}\right) \tag{3}$$

$$\frac{P'}{P} = \left(\frac{N'}{N}\right)^3\left(\frac{D'}{D}\right)^5\left(\frac{\rho'}{\rho}\right) \tag{4}$$

$$\eta_{sF}{}' = \eta_{sF} \tag{5}$$

where $\dot{V}$ is the fan volume flow rate, N is the fan running speed, D the fan diameter, Δp_{sF} is the fan static pressure rise, ρ is the inlet air density and P is the fan shaft power. The use of the fan scaling laws is however based on the premise that dynamic similarity exists between the model and full scale prototypes. This requires the Reynolds numbers of the model and full scale prototypes to be identical. The fan Reynolds numbers is defined as:

$$Re_{fan} = \frac{\rho V_{fan} L}{\mu} \tag{5}$$

where V_{fan} is the velocity of the blade at a specified radius, defined as:

$$V_{fan} = \frac{2\pi N r}{60} \tag{6}$$

and L is the chord length of the fan blade at a specific radius. Due to limitations on the size of available test facilities and structural limitations on the materials used for blade manufacture (limiting the running speed) it is not possible to have identical Reynolds numbers when testing large diameter axial flow fans. The tip Reynolds number of the 1.25 m diameter fan, running at a speed of 900 RPM is in the order of 6.0×10^5, while the tip Reynolds number for the 10.36 m diameter fan, running at a speed of 110 RPM is in the order of 4.5×10^6. The Reynolds number (based on blade chord) for both fan diameters can therefore be classified as falling in the “fully turbulent” regime.

EXPERIMENTAL FANS

Figure 2 and Figure 3 show the two fans used for the study. The L-fan has 8 blades with a rotor diameter of 1.24 m, a hub/tip ratio of 0.135 and chord length of 150 mm. The 9 blade N-fan has the same rotor diameter and hub/tip ratio as the L-fan but is characterised by a smaller chord length of 90 mm and lower solidity. The casing diameter of both fans is 1.25 m, resulting in a tip clearance of 5 mm. These fans were specifically selected as it represents models of fans that would typically be used in ACSC installations.

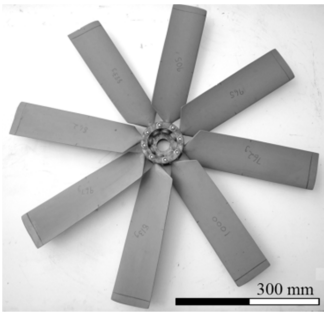

Figure 2 - L-fan

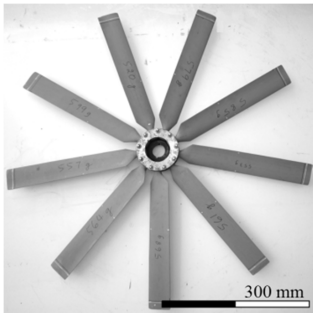

Figure 3 - N-fan

No geometric models were available for either of the fans and therefore the scaled models were three-dimensionally scanned to obtain the geometries for use in the numerical simulations. A contact scanner was used to generate a three-dimensional point cloud for the geometry of each fan. Each probe started at the trailing edge of the blade suction side, following the geometry around to the trailing edge of the pressure side. This ensured that the leading edge of each radial profile was accurately scanned. This procedure was repeated for multiple radii in the span-wise direction. The point cloud of the L-fan is shown in Figure 4.

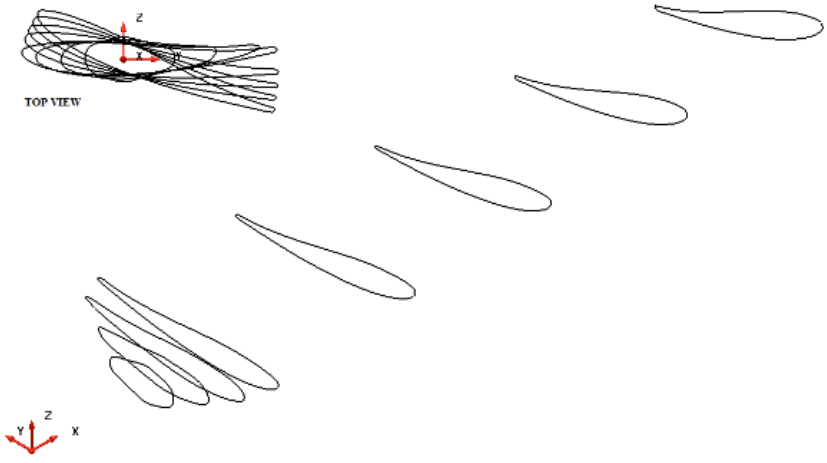

Figure 4 - Point cloud of the geometry of the L-fan

The scanning procedure proved to be time consuming and expensive and consequently only 8 radially spaced blade profile probe traces were carried out. A surface for each point cloud was created using a lofting function through the set of eight scanned blade profiles for both the L- and N-fan. The final geometrical model of the L-fan (left) and N-fan (right) is shown in Figure 5.

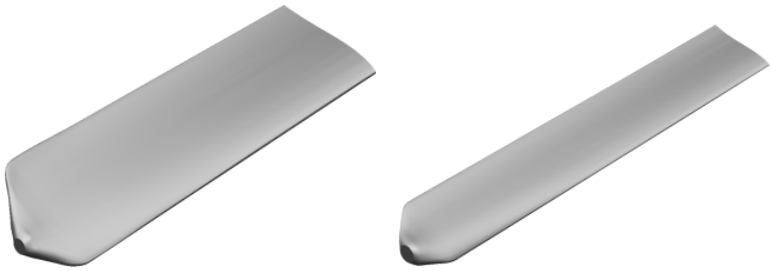

Figure 5 - Geometric model of the L-fan (left) and N-fan (right)

EXPERIMENTAL TESTS

All experiments were conducted on the large fan test facility situated at the University of Stellenbosch's Department of Mechanical & Mechatronic Engineering. The specifications of the facility are based on the BS 848 standards for axial flow fans, type A. The main features of the facility shown in Figure 6 are:

1. A calibrated bell mouth inlet used to measure the volume flow rate through the fan.
2. A manual throttle unit with louvres used to adjust the volume flow rate through the test facility.
3. An axial booster fan to overcome the flow resistance induced by the front tunnel-end of the facility. The booster fan enables measurements to be taken at low pressure rise, high volume flow rate operating points.
4. A flow straightener to remove swirling flows and eddies induced into the flow field by the booster fan.
5. Guide vanes and three mesh screens of increasing fineness are situated inside the settling chamber (6) to ensure a more uniform velocity profile and distribution of air entering the inlet of the fan.
6. A settling chamber (4 m high, 4 m wide and 7 m long) to slow down the inlet flow velocity into the fan to such an extent that the dynamic pressure at fan inlet is considered to be negligible (the velocity is smaller than 2 m/s). The large dimensions of the settling chamber relative to the test fan diameter ensure that the fan inlet is considered to be "open".
7. The test fan(s) with rotor diameter of 1.24 mm situated inside the bell mouth with a diameter 1.25 m.
8. The test fan drive unit. The fan is driven by a 10 kW electric motor controlled by a variable speed drive. The torque transducer is positioned between the fan and the pulley at the end of the drive shaft.

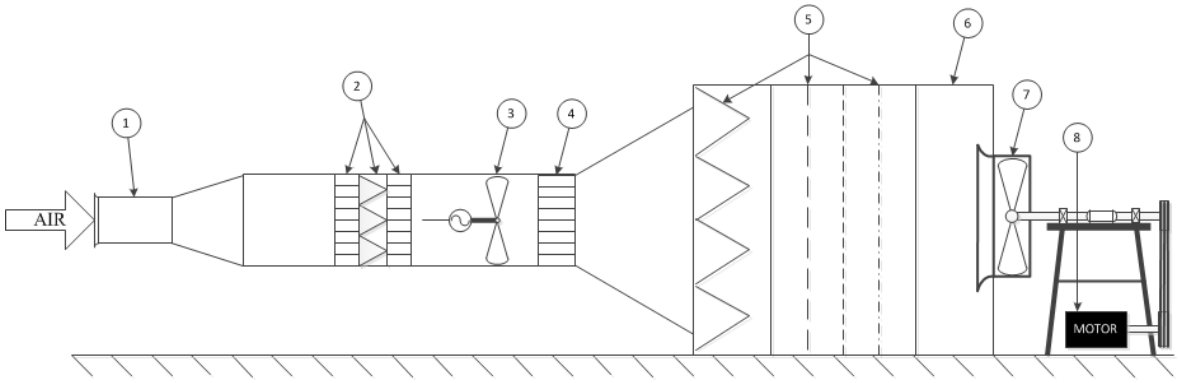

Figure 6 - Type A, BS 848 test facility

Static pressure measurements p_{sF} were taken at the bell mouth inlet, to determine the volume flow rate $\dot{V}$, and at the settling chamber p_{sett} to determine the fan static pressure rise. Pressure measurements were performed using two 1000 Pa PD1 HBM inductive pressure transducers. The fan shaft torque T was determined using a 100 Nm T22 HBM, static calibrated, torque transducer. The rotational speed N of the fan was determined using a proximity switch and a frequency to voltage converter.

To calculate the fan static pressure p_{sF}, fan shaft power P, and fan static efficiency η_{sF}, the following formulations, in accordance with the BS 848 standards, were used:

$$p_{sF} = p_{amb} - (p_{sett} - p_{dsett}) \tag{6}$$

$$P = \frac{2\,\pi\,N\,T}{60} \tag{7}$$

$$\eta_{sF} = \frac{p_{sF}\dot{V}}{P} \tag{8}$$

All test results were referenced to values of 1.2 kg/m³ and 900 RPM using the fan scaling laws. Repeatability tests that were performed on the facility showed the repeatability of fan static pressure value results to be within 2%.

NUMERICAL MODELLING

The geometry that was used in the simulations represented the BS 848 type A test facility detailed in the previous section. A lay-out of the geometry is shown in Figure 7 where D_h is the hydraulic diameter, calculated using the diameter D of the fan.

The computational mesh was sub-divided into three sections: an inlet, blade passage and an outlet. ANSYS *TurboGrid* was used to generate a structured mesh and ANSYS *Fluent* was used to solve the simulations. Periodicity was used to reduce the computational domain to only an 8^{th} (L-fan) or 9^{th} (N-fan) of the size which made greater local refinement of the mesh grid possible. All simulations used a steady state, multiple rotating reference frame, approach. The realizable k-ε turbulence model together with enhanced wall treatment [7] was used. The inlet turbulence boundary conditions for the small fans were set to an intensity value of 3% and hydraulic diameter of 4.1 m respectively. For the large fans these values were set to 2.3% and 21 m respectively.

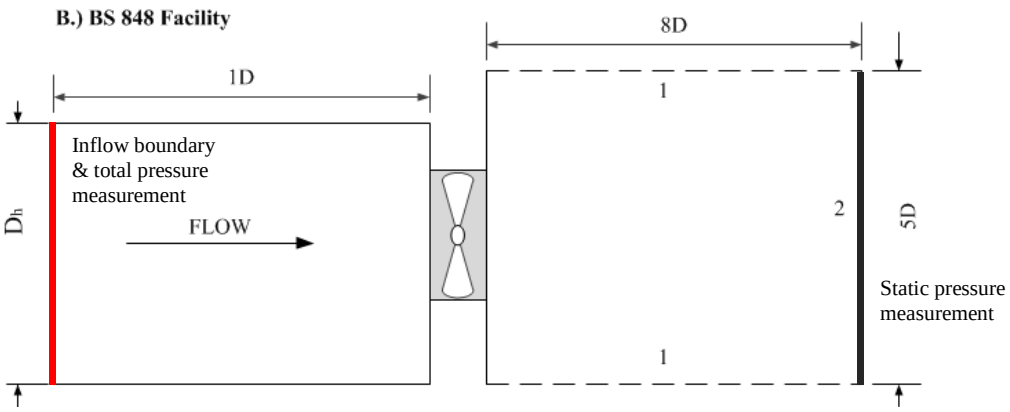

Figure 7 - Mesh configuration used for numerical study

The choice of the pressure-velocity coupling method was based upon the use of the SIMPLE algorithm by other authors [4,5,8,9]. The QUICK scheme was used for discretization purposes. It is specifically useful in swirling and rotating flows and regarded as a higher-order discretization scheme which is typically more accurate than a second-order upwind scheme for structured meshes with cell faces aligned with the flow [7,10]. In comparison to the second-order upwind scheme, improved convergence for the simulations was found specifically when using the QUICK scheme.

Computational resources for modelling purposes, which include mesh generation and post-editing, used a 2.5 GHz quad-core processing unit and 8 GB RAM. Case files were solved on a computational cluster with a capability of up to 16 CPU units per case.

The computational domain resembles the BS 848 test facility shown in Figure 8. The large, but shortened (compared to the actual BS 848 test facility), inlet contained an inlet bell mouth. Due to a relative coarse inlet domain, the cells in the bell mouth region were locally refined to ensure appropriate near-wall spacing.

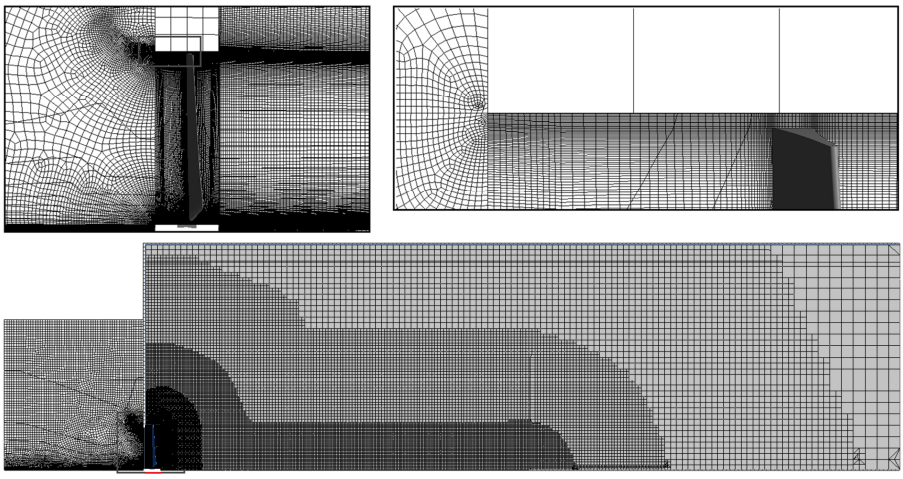

Figure 8 - Computational mesh

In order to simulate a fan-to-open atmosphere setup, a large outlet domain was required. To prevent an excessive mesh size the mesh was grown towards the outer boundaries of the domain. The mesh of the L-fan contained 1.2 million cells and the mesh of the N-fan contained 2.8 million cells. A mass flow condition for the inflow boundary was specified. The periodic boundary faces labelled (1) and outlet face (2) in Figure 7 were all specified to have pressure outlet boundary

conditions. A no-slip condition was applied to all walls i.e. the settling chamber and fan walls. Large amounts of back flow were expected at the outer boundaries (see Figure 7) which would affect the stability and speed of convergence of the simulations.

Large scale simulations of the L- and N-fans were performed by scaling these fan geometries to a diameter of 10.36 m and using the same solver settings as detailed above. The results of the mesh dependence study are shown in Table 1. Each fan configuration had to be meshed separately. The smallest mesh size that gave a stable answer (no cyclic variation) for the predicted fan static pressure was selected as the mesh size for the simulations (these are highlighted in grey). The corresponding rotor section mesh is also indicated for these meshes.

Table 1 - Mesh dependence study

L-fan 1.25 m			N-fan 1.25 m			L-fan 10.36 m			N-fan 10.36 m		
Mesh	Rotor mesh	ΔpsF	Mesh	Rotor mesh	ΔpsF	Mesh	Rotor mesh	ΔpsF	Mesh	Rotor mesh	ΔpsF
925075		123.1	929597		104	1434253		128	1174546		103.9
1170805	616162	122.9	2787420	2292756	109.3	1727246	922254	126.8	1406375	743559	103.4
1676907		122.7	3949744		109	2488452		127	2035958		103.6

RESULTS

The solutions were considered to be converged if all residuals reached a tolerance value of 10^{-5} and the monitored parameters (total inlet pressure and static outlet pressure – see Figure 7) remained constant for increasing iterations. The large computational domain resulted in some simulations only converging after 45-50 hours.

The L-fan was simulated for the design blade-setting angle of 6.9 degrees and the N-fan was simulated for a blade setting angle of 12 degrees. The fan static pressure was calculated as the differences between the area-averaged total pressure at the inlet and area-averaged static pressure at the outlet. Figure 9 compares the experimental and numerical results of the fan static pressure for both fans.

In the case of the L-fan good agreement with experimental results was found for the entire flow rate region, except at a 0 m^3/s. The largest percentage pressure deviation is 7% at 10.18 m^3/s (ignoring the 0 m^3/s point). Similar correlation between numerical and experimental values was found in the case of the N-fan. If the 0 m^3/s point is ignored, the largest percentage deviation in pressure is 7% at 7 m^3/s.

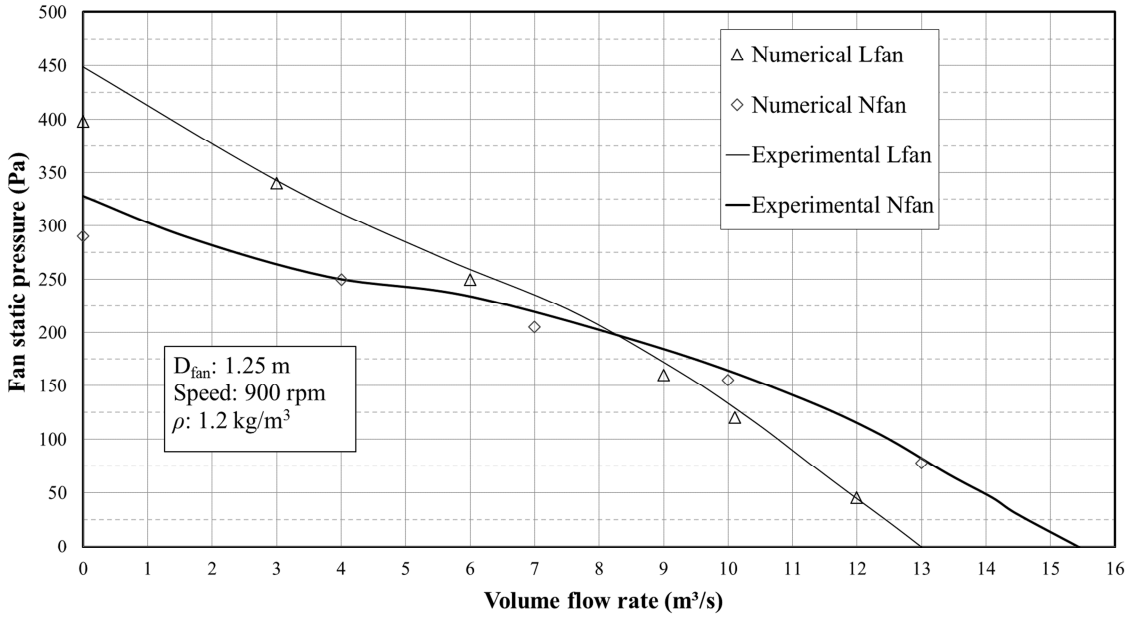

Figure 9 - Fan static pressure for the 1.25 m diameter L-fan and N-fan

The results for fan shaft power of the L- and N-fan show good agreement overall. Figure 10 shows that the fan power is slightly under-predicted for all operating points of both fans. Besides the larger deviation at 0 m^3/s, which is expected, the largest percentage deviation for both approaches is below 8 %.

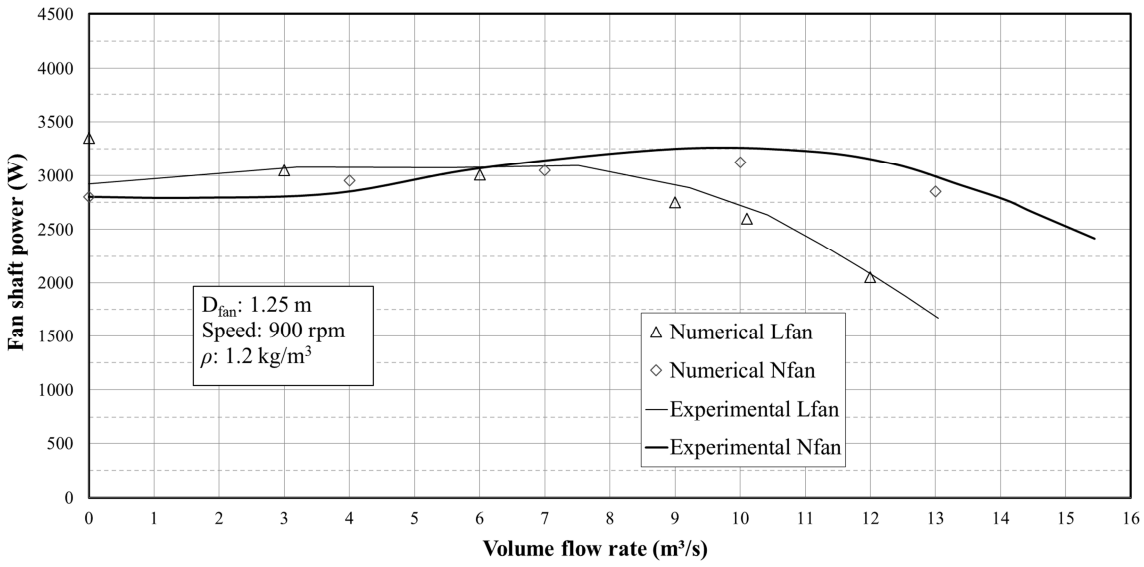

Figure 10 - Fan shaft power for the 1.25 m diameter L-fan and N-fan

Both the calculated fan static pressure and fan shaft power correlates well with the experiments. Moreover, due to the slight under-estimation of both these parameters, an even better correlation can be expected for the fan static efficiency (see Fig. 11). In fact, the L-fan and N-fan's static efficiency results are only slightly (~2.0 %) under-predicted.

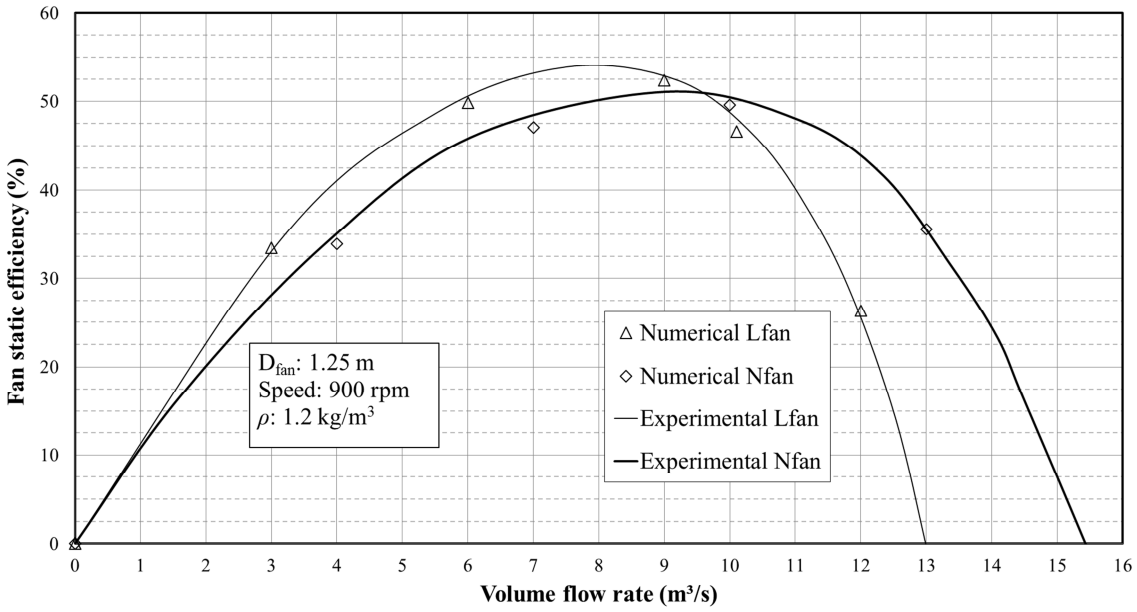

Figure 11 - Fan static efficiency for the 1.25 m diameter L-fan and N-fan

Figure 12 shows the fan static pressure results of the large diameter fan simulations, compared to the scaled experimental results for a diameter of 10.36 m and speed of 107 RPM using the fan scaling laws. The numerical results correlate very closely with the experimental data for both the L- and N-fans.

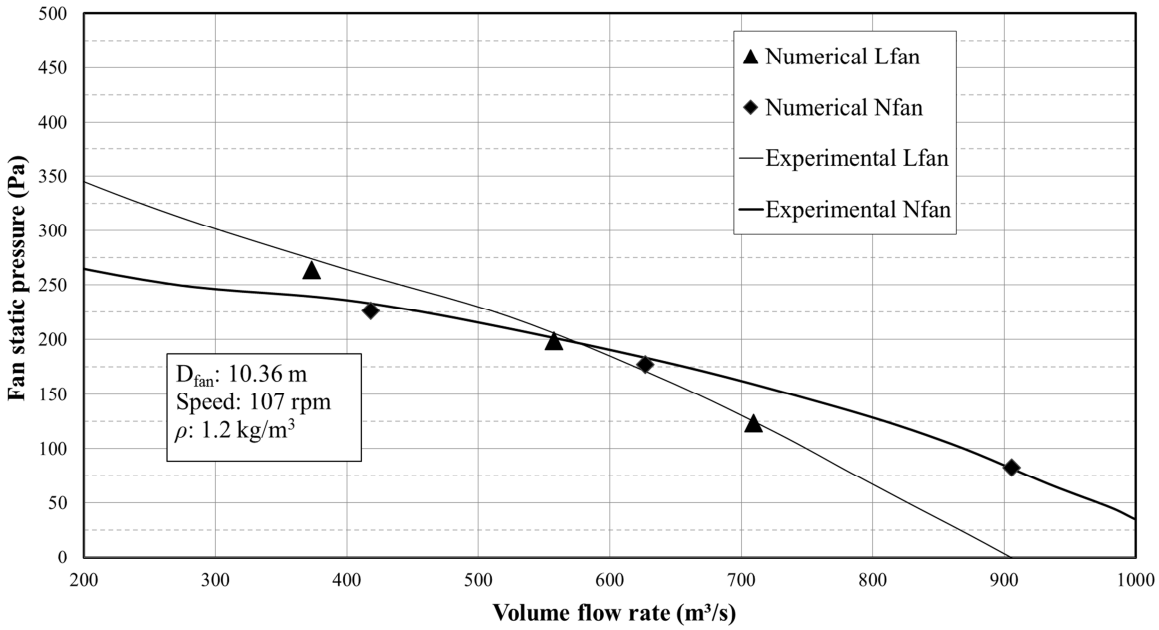

Figure 12 - Fan static pressure for the 10.36 m diameter L-fan and N-fan

Figure 13 shows the scaled fan shaft power results. The numerical results for both the L- and N-fans are about 10% lower than the scaled experimental results.

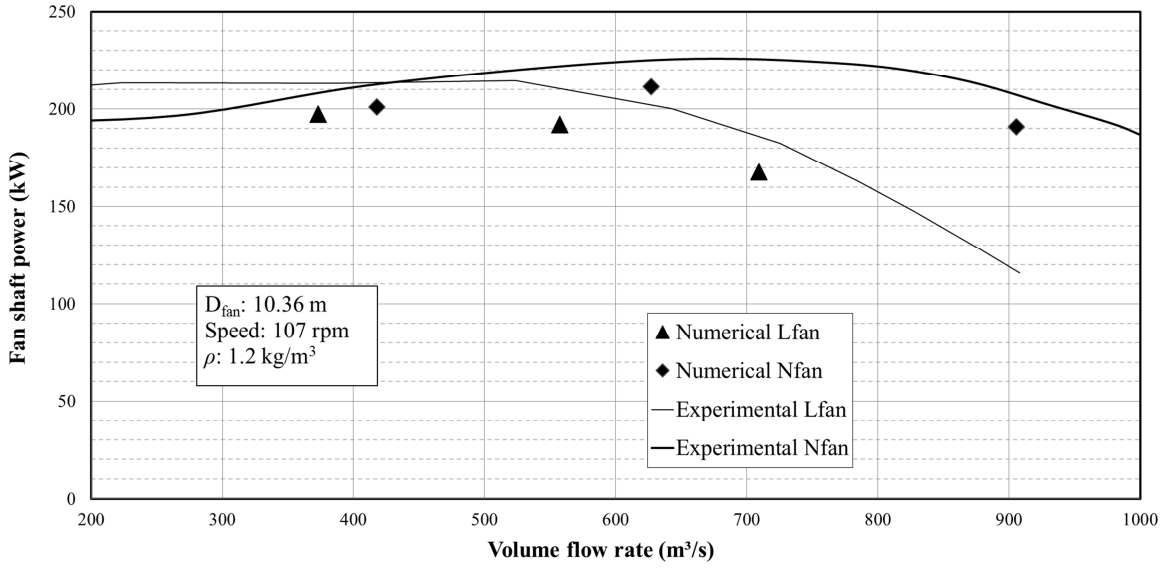

Figure 13 - Fan shaft power for the 10.36 m diameter L-fan and N-fan

For the large diameter fan efficiency results the efficiency values themselves are between 5 % (L-fan) and 2 % (N-fan) higher than the efficiency for the scaled experimental fans.

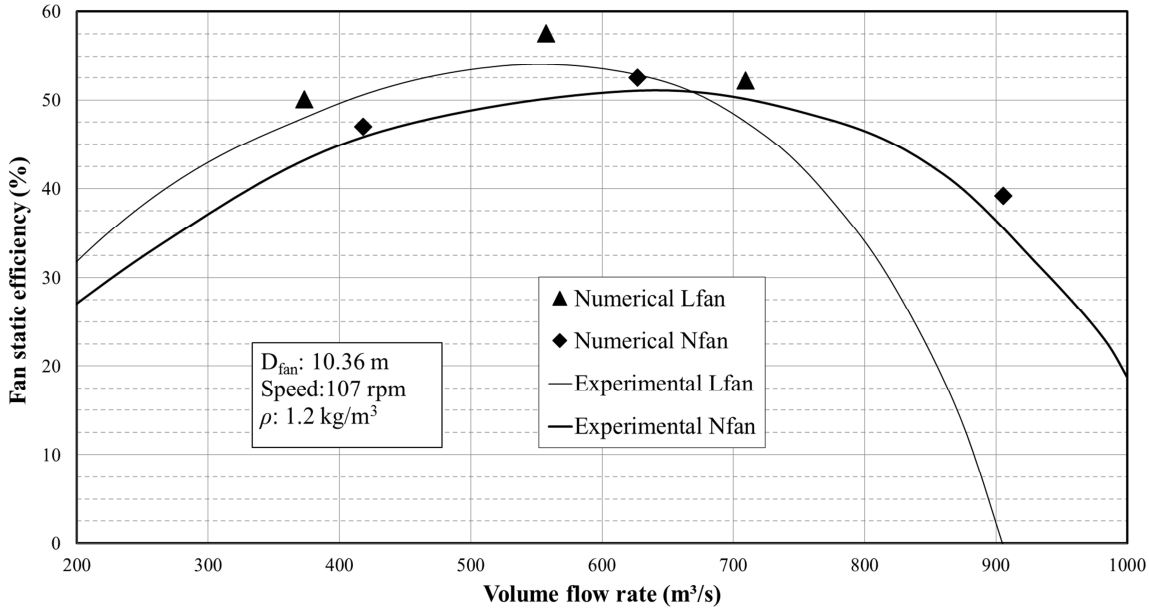

Figure 14 - Fan static efficiency for the 10.36 m diameter L-fan and N-fan

CONCLUSION

The L- and N-fan were numerically simulated using a steady state, multiple rotating reference frame approach and validated by experimental test results. The good agreement of the 1.25 m diameter L- and N-fan's numerical results with the respective experimental results validates not only the numerical results but the methodology and approach for both fan configurations. It should be noted that these correlations were obtained using the realizable k-ε turbulence model, which is considered appropriate for the simulation of fully turbulent flow [11] (the tip Reynolds number of the experimental fans is in the order of $5x10^5$). Considering that the large 10.36 m diameter fans were

simulated at a much tip higher Reynolds number, the use of the realizable k-ε turbulence would therefore be appropriate for these fans as well.

The CFD fan static pressure CFD results of the large 10.36 m diameter L- and N-fans correlate well with the scaled experimental results. The shaft power results differ from the scaled experimental results by being about 10 % lower. The consequence of this is that the fan static efficiency values of the large diameter L- and N-fans are between 2 and 5 % higher than the scaled experimental results. This is expected since it is generally accepted that higher Reynolds number flows correlate with lower friction coefficients and consequently higher efficiencies.

The good correlation of the scaled results differ from the findings of Meyer and Kröger in that they found differences for both the scaled fan static pressure and shaft power results and consequently very close correlation for the fan static efficiency results. It should however be noted that the results of Meyer and Kröger are closely linked to the 2-dimensional properties of the fan blade profiles used in their actuator disc simulations. Compared to the actuator disc model used by Meyer and Kröger, the fully detailed CFD simulation performed in this investigation include 3-dimensional flow effects like radial flow, tip clearance and hub/blade interaction that are not present in the model of Meyer and Kröger.

This investigation considered the application of the fans scaling laws to large diameter fans in the fully turbulent flow regime (based on fan blade chord). The results show that, without compensating for the effect of Reynolds number, the fan scaling laws predict fan efficiency within 5% of expected fan performance values.

REFERENCES

[1] Kröger, D.G., 2004, Air-cooled Heat Exchangers and Cooling Towers, PennWell Corporation, Tulsa.

[2] Augustyn O.P.H., 2013, “Experimental and Numerical Analysis of Axial Flow Fans,” University of Stellenbosch.

[3] Bredell J., Kröger D. G., and Thiart G., 2006, “Numerical investigation of fan performance in a forced draft air-cooled steam condenser,” Applied Thermal Engineering, 26(8-9), pp. 846–852.

[4] Zhao W., Qu Q., and Li Q., 2012, “Numerical investigation on the flow field of an axial flow fan in a direct air-cooled condenser for a large power plant,” Heat Transfer-Asian Research, (51039004), p. n/a–n/a.

[5] Meyer C.J., Kröger D.G., 2004, “A Numerical Investigation of the Errors Associated with the Scaling of Axial Flow Fan Performance Characteristics,” R&D Journal, Volume 20 (2).

[6] Pelz P.F., Stonjek S., Matyschok B., 2012, "The Influence of Reynolds number and Roughness on the Efficiency of Axial and Centrifugal Fans - a Physically Based Sclaing Method", Proceedings of FAN 2012 conference, France.

[7] ANSYS Fluent, 2011, ANSYS Inc. - Fluent theory guide.

[8] Fernandez Oro J. ., Arguelles Diaz K. ., Santolaria Morros C., and Galdo Vega M., 2011, “Numerical simulation of the unsteady stator-rotor interaction in a low-speed axial fan including experimental validation,” International Journal for Numerical Methods for Heat & Fluid Fllow, 21(2), pp. 168–197.

[9] Masi M., and Lazzaretto A., 2012, “CFD models for the analysis of rotor-only industrial axial-flow fans,” Proceedings of FAN 2012 conference, France.

[10] Versteeg H. K., and Malalasekera W., 2007, An Introduction to Computational Fluid Dynamics: The Finite Volume Method, Pearson, Harlow.

[11] Shih, T.H., William, W.L., Shabbir, A., Yang, Z., Shu, J., 1995, "A new K-ε eddy viscosity model for high Reynolds number turbulent Flows", Computers Fluids, 24 (3).